Scientific Reports

https://doi.org/10.1038/s41598-025-32611-9

Article in Press

FeBTC as peroxidase mimic for colorimetric cholesterol detection

Received: 11 September 2025

Accepted: 11 December 2025

Published online: 26 December 2025

Cite this article as: Abed H., Sabouni R., Ghommem M. *et al.* FeBTC as peroxidase mimic for colorimetric cholesterol detection. *Sci Rep* (2025). https://doi.org/10.1038/s41598-025-32611-9

Heba Abed, Rana Sabouni, Mehdi Ghommem, Muhammad Umar Azam, Khalid Askar & Nouha Alcheikh

FeBTC as Peroxidase Mimic for Colorimetric Cholesterol Detection

Heba Abed[1], Rana Sabouni[1,2*], Mehdi Ghommem[3*], Muhammad Umar Azam[4], Khalid Askar[4], Nouha Alcheikh[4]

[1]Biomedical Engineering Program, Department of Chemical and Biological Engineering, American University of Sharjah, Sharjah, UAE
[2]Department of Chemical and Biological Engineering, American University of Sharjah, Sharjah, UAE
[3]Department of Mechanical Engineering, American University of Sharjah, Sharjah, UAE
[4]Department of Mechanical and Nuclear Engineering, Khalifa University of Science and Technology, Abu Dhabi, UAE

Corresponding authors:
Mehdi Ghommem, Department of Mechanical Engineering, American University of Sharjah, Sharjah, UAE.
Email: mghommem@aus.edu

Rana Sabouni, Department of Chemical and Biological Engineering, American University of Sharjah, Sharjah, UAE
Email: rsabouni@aus.edu

Abstract

Cholesterol sensing is essential for the early detection of several diseases such as hypercholesterolemia, atherosclerosis, and cardiovascular disorders. To address the limitations of enzyme-based methods, this paper proposes a novel Metal Organic Framework (MOF)-based spectrophotometric platform for cholesterol detection. Iron-based MOF (Fe-BTC) is introduced as a novel, peroxidase mimic nanozyme for cholesterol detection. Characterization studies run on Fe-BTC, including Fourier transform infrared spectroscopy, X-ray diffraction, and zeta potential, revealed its stable, amorphous nature and potential peroxidase activity due to Fe centers. Parametric studies including pH, time, temperature, and reagent concentrations were performed to determine operating conditions for H_2O_2 and cholesterol detection. Mechanistic studies demonstrated biosensor operation via $OH^{\cdot}$ radical formation by Fe-BTC. The present biosensor achieved a cholesterol limit of detection (LOD) of 2.91 µM and 2.88 µM at 25 ºC and 37 ºC cholesterol incubation, respectively, with a linear detection range of 6.56–78.75 µM at both temperatures. The biosensor had good selectivity to cholesterol in the presence of interfering analytes, including glycine, uric acid, glucose, and NaCl. Overall, our novel Fe-BTC-based biosensor demonstrated comparable performance to nanomaterial-based cholesterol sensors reported in the literature, with a simpler, cheaper, and scalable design, and shows great promise for cholesterol detection via spectrophotometric methods.

Keywords : Cholesterol, Fe-BTC, Limit of Detection (LOD), Metal Organic Framework (MOF), Colorimetric, Sensor, Detection, Nanozyme.

1. Introduction

Cholesterol is an essential biomolecule and biomarker used to characterize human health. It has active roles in maintaining cell membrane integrity, metabolite and hormone synthesis, cell signalling, and other cellular functions [1–3]. However, excess cholesterol levels in the blood is associated with detrimental health effects, including cardiovascular diseases, chronic ischaemia in retinal tissues, atherosclerosis, chronic kidney diseases, among others [3–6]. Elevated cholesterol levels is a prevailing problem in the United States, with approximately 86 million adults registering cholesterol levels above 200 mg/dL, as of the Centers for Disease Control and Prevention (CDC) 2020 reports [7]. Thus, continuous monitoring of cholesterol levels is necessary for early diagnosis and treatment, especially in high-risk patients. Traditionally, cholesterol levels are quantified using the cholesterol oxidase/peroxidase/4-aminophenazone (CHOD-POD-PAP) method in clinics, which involves the use of horseradish peroxidase (HRP) [8]. HRP is known for its low stability and sensitivity to temperature changes, limiting the method with added costs and time [8].

Artificial enzymes, also coined nanozymes, have emerged as stable nanomaterials that mimic enzyme activity, offering higher stability, lower cost, and easier handling [9,10]. Magnetic nanoparticles, Metal Organic Frameworks (MOFs), nanowires, quantum dots, and others have been used as peroxidase mimics to replace HRP [10]. Among these, MOFs stand out for their high surface area, tunable structure, and catalytic activity, making them promising candidates for cholesterol sensing [8,9]. To date, many MOFs and hybrid-MOF nanomaterials have been used as peroxidase mimics for spectrophotometric cholesterol detection. For example, MIL-101(Cr) was adopted as a peroxidase mimic for colorimetric cholesterol detection, achieving limit of detection LOD of 0.86 μM and a linear detection range of 1.1 – 22.9 μM [11]. Meanwhile, other studies adopted hybrid MOF-based sensors for improved cholesterol sensing and peroxidase activity. For instance, MIL-100(Fe)-coated Fe_3O_4 magnetic nanoparticles were synthesized for cholesterol detection, achieving a wider linear detection range of 2 – 50 μM, and similar LOD at 0.8 μM [12]. Other hybrid nanomaterials include GQDs/UiO-66 [13] and Pd@ZIF-8 [14]. However, many of these sensors are limited by low dynamic ranges, prolonged sensing time, and high production costs, leaving room for improvement. In this context, Fe-BTC offers a simpler and more economical alternative.

Fe-BTC, commercially available as Basolite F300, is a promising MOF with high potential for effective peroxidase activity. Fe-BTC consists of iron-based metal centers linked with 1,3,5-benzenetricarboxylic acid (BTC) organic linkers [15,16]. Iron mainly exists in the Fe(III) oxidation state and demonstrates an amorphous nature, with poor crystallinity. This amorphous and irregular structure may provide a larger number of exposed active sites, enhancing peroxidase activity and enabling faster, more sensitive detection [17] Fe-BTC also exhibits high biocompatibility, low toxicity, and intrinsic catalytic activity, making it a promising candidate for nanozyme applications [15,16].

In this work, Fe-BTC is proposed as a novel, peroxidase-mimic nanozyme for colorimetric detection of cholesterol. Current literature reports the usage of other Fe-based MOFs, including MIL-101(Fe) [18], MIL-53(Fe) [19], and MIL-100(Fe) [12], often functionalized with other nanomaterials. To the best of our knowledge, this is the first report on the use of Fe-BTC alone as a peroxidase-mimic nanozyme for colorimetric cholesterol detection. Comprehensive characterization was conducted to determine the structural, physical, and chemical properties

of Fe-BTC. Characterization tests involved Fourier Transform Infrared (FT-IR), X-ray Spectroscopy (XRD), Scanning Electron Microcopy (SEM), Energy Dispersive X-ray Spectroscopy (EDS), X-ray Photoelectron Spectroscopy (XPS), and zeta potential. This was followed by parametric studies of different variables to test Fe-BTC peroxidase activity for H_2O_2 detection using 3,3',5,5'-tetramethylbenzidine (TMB) dye. Such variables tested include pH, incubation time, and both Fe-BTC and TMB concentrations. Then, using cholesterol oxidase enzyme, cholesterol detection operating conditions are chosen through parametric studies and the sensor's performance, such as its sensitivity and selectivity, is evaluated. The selectivity was tested against multiple interferents, including glucose, sucrose, glycine, L-cystiene, NaCl, and others. Due to Fe-BTC's commercial availability, low costs, and simple, non-hybrid nature, Fe-BTC shows great promise for use in cholesterol sensors and integration into point-of-care (PoC) devices.

2. Experimental Methodology

2.1 Materials

Cholesterol (>99% purity), 3,3',5,5'-tetramethylbenzidine (TMB) (≥99%), ethanol, tert-butyl alcohol, 37% hydrochloric acid (HCl), and sodium hydroxide (NaOH) were obtained from Sigma-Aldrich and used without further purification. Fe-BTC was purchased under the trademark Basolite F300 from Sigma Aldrich. Hydrogen peroxide (35%) was purchased from Sigma Aldrich and diluted to 10 mM using distilled water before use. Cholesterol Oxidase (ChOx) ex. Microorganism, 10U/mg powder 2500 Units was purchased from Sisco Research Laboratories. Phosphate Buffered Saline (PBS) capsules were purchased from Sigma Aldrich and dissolved in 200 mL distilled water to form PBS buffer solution; pH was adjusted with NaOH or HCl according to need. TMB was dissolved in ethanol to form 10 mM solution, which was used in all experiments. Glycine (≥98.5%), L-cysteine (97%), L-lysine (≥98%), urea (99.0-100.5%), uric acid (≥99%), glucose, sucrose, fructose, sodium chloride (NaCl), potassium chloride (KCl), and calcium chloride ($CaCl_2$) were purchased from Sigma Aldrich and used for selectivity studies.

2.2 Instrumentation and Methods

Various instruments were used for characterization and experimentation. A FEI Nova NanoSEM 650 was used to collect FE-SEM images. Before analysis, gold coating (around 10 nm) was deposited. Images were taken at 100 µm and 1 nm magnification. A PANalytical Empyrean equipped with high-resolution optics and detectors (PIXcel3D) and Cu Kα radiation. was used to collect X-ray diffraction (XRD) patterns. The scan parameters included a 2θ range of 4 to 80 degrees, a voltage of 45 kV, and a current of 40 mA. Fourier Transform Infrared Spectroscopy (FT-IR) measurements were taken using Perkin Elmer Spectrum 3 FT-IR Spectrometer. X-ray photoelectron spectroscopy (XPS) measurements were taken using Escalab Xi+ by Thermo Scientific Fischer, equipped with a monochromatic Al Kα X-Ray source and a high-resolution hemispheric electron energy analyzer for precise energy measurements. Zetasizer Blue Lab (Malvern Panalytical) was used for zeta potential determination, whereby samples were dispersed in deionized water, sonicated, then analyzed. Thermo Scientific Fischer Phenom Workstation was used for electron mapping via Energy-dispersive X-ray spectroscopy (EDS).

Absorption measurements were collected using a Shimadzu UV-2600i UV-VIS spectrophotometer at the wavelength range 350 – 800 nm. pH measurements were performed using a Thermo Fisher Scientific Orion Star A111 pH meter. Mass measurements were collected using a Shimadzu ATY224 electronic balance. Centrifugation was performed using a Hettich Mikro 220 Benchtop centrifuge, while shaking was achieved using a Fisher Brand Incubating Mini Shaker. Sonication of samples was conducted using a MH-020G Ultrasonic Cleaner.

2.3 Overview of the Proposed Cholesterol Detection Method

The biosensor proposed involves using Fe-BTC as a MOF-based nanozyme functioning as a peroxidase mimic, as illustrated in Figure 1. First, cholesterol is incubated separately in ChOx to break cholesterol into cholest-4-ene-3-one and hydrogen peroxide (H_2O_2). Subsequently, Fe-BTC and TMB dye are added to the mixture to react with the produced H_2O_2. Specifically, H_2O_2 is reduced by Fe-BTC while TMB is oxidized and forms a TMB/diamine charge complex,

leading to a color change from colorless to blueish green. The intensity of color change is correlated to the concentration of H_2O_2 produced and cholesterol being initially present.

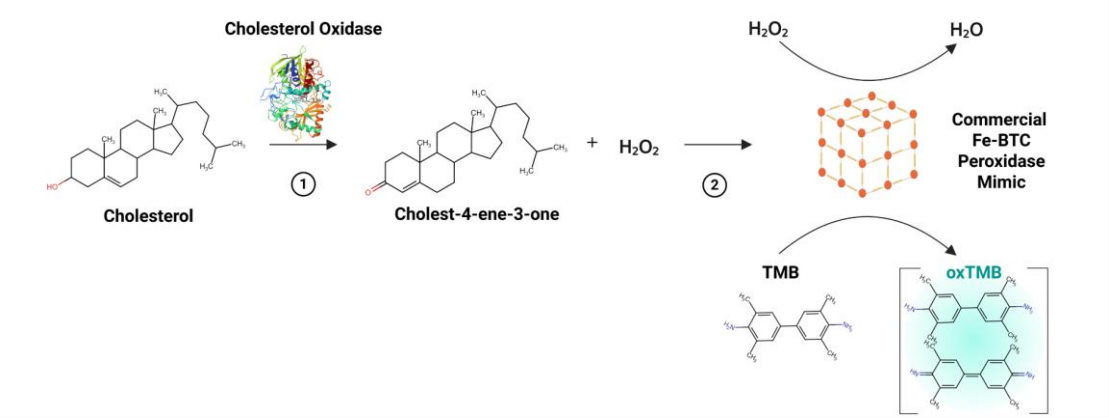

Figure 1: Overview of cholesterol detection using Fe-BTC as a peroxidase mimic.

The experimental procedures used to develop and test the Fe-BTC biosensor proposed as a peroxidase mimic for cholesterol detection involve two main steps. First, the system is tested to determine the best operating conditions for H_2O_2 detection by Fe-BTC, and the LOD for H_2O_2 is determined. Various experiments are run to discern the mechanism of H_2O_2 detection by the Fe-BTC-based peroxidase system. Next, cholesterol incubation with ChOx is evaluated through paramateric studies, followed by testing cholesterol detection by the full Fe-BTC-TMB sensing system, analyzing biosensor performance, and calculating the limit of cholesterol detection (LOD). Finally, selectivity tests against interferents are investigated.

2.4 H_2O_2 Detection using Fe-BTC-TMB system

To determine the limit of detection of H_2O_2 using Fe-BTC, different H_2O_2 concentrations were added to the MOF, and the absorbance was measured to quantify the resulting color change. 400 µM H_2O_2 was used to prepare solutions with low H_2O_2 concentrations (0.0 – 100.0 µM) while 10 mM H_2O_2 stock solution was used for preparing high H_2O_2 concentrations (100.0 – 1000.0 µM). 375 µL of 4 mg/mL Fe-BTC and 600 µL of 10 mM TMB were added to multiple Eppendorf vials. Then, varying volumes of 400 µM or 10 mM H_2O_2 solution were added to the vials and made up to 2 mL with PBS (pH = 5.0) to form H_2O_2 concentrations ranging from 0.0 – 1000.0 µM. The solutions were incubated for 50 mins with 800 rpm shaking in dark conditions, after which they were centrifuged at 12000 rpm for 5 mins. The supernatant was collected, and the TMB concentrations were determined using a UV-Vis spectrophotometer at 660 nm, with absorbance measured from 400 nm to 800 nm. Triplicate solutions were made for each H_2O_2 concentration tested, for average and standard deviation calculations, represented in error bars. Figure 2 illustrates the overall experimental procedure described above followed for all H_2O_2 detection studies, outlining solution preparation, shaking, centrifugation, and absorption measurements. A plot of absorbance against H_2O_2 concentration is generated, and the limit of detection (LOD) is calculated according to the standard deviation and slope of the linear portion using Equation (1) [20]:

$$\mathrm{LOD} = 3.3\,\frac{\sigma}{m} \qquad (1)$$

where σ is the standard deviation of the response and m is the slope of the calibration curve. The standard deviation of the response is calculated by determining the standard deviation of the y-intercept of the regression line ($S_{y/x}$).

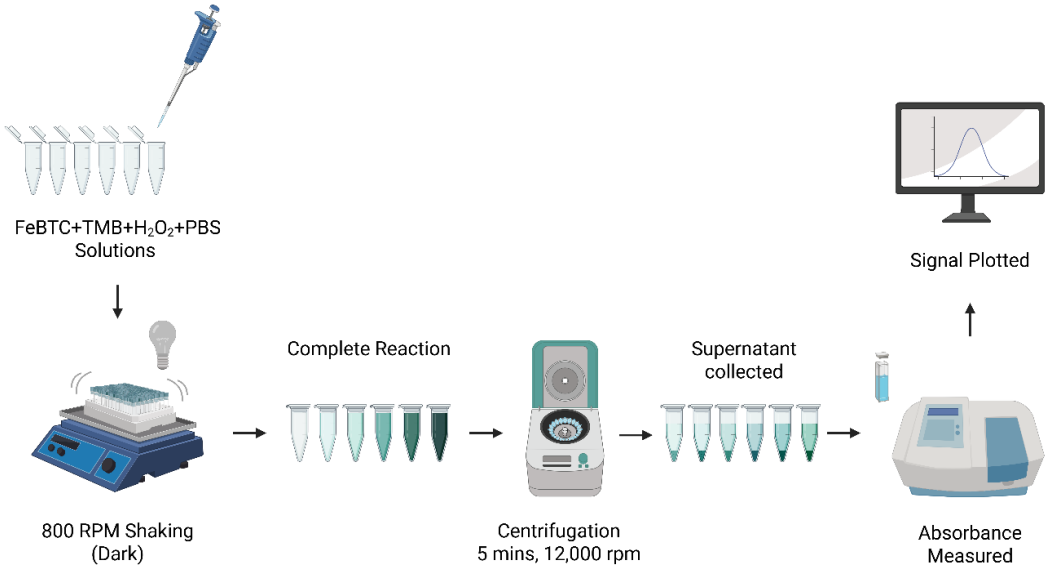

Figure 2: General experimental protocol for H_2O_2 detection studies.

2.6 Fe-BTC Peroxidase Activity and H_2O_2 Detection Mechanism

To understand the Fe-BTC peroxidase action and H_2O_2 detection by the Fe-BTC-TMB sensing system, multiple experiments were carried out. These include measuring the absorbance of all system components and combinations, determining H_2O_2 radicals produced by Fe-BTC peroxidase using tert-butyl alcohol, and understanding Fe-BTC's adsorption of TMB dye. These protocols are detailed below.

2.6.1 Peroxidase System Components & Interactions

To investigate the peroxidase activity of Fe-BTC and the contribution of each component of the Fe-BTC-TMB system to the peroxidase activity, a series of control experiments were performed. Specifically, 2 mL solutions of PBS (pH = 5.0), TMB, Fe-BTC, H_2O_2, TMB+ H_2O_2, Fe-BTC+ H_2O_2, Fe-BTC+TMB, and Fe-BTC+TMB+H_2O_2 were prepared in Eppendorf vials using pH 5.0 PBS solvent. Concentrations of each reagent were kept constant across the samples, matching the operating conditions identified previously: TMB at 3 mM (600 µL of 10 mM TMB stock solution in ethanol), 0.75 mg/mL Fe-BTC (375 µL of 4 mg/mL stock Fe-BTC solution) and 100 µM H_2O_2 (20 µL of 100 mM stock). To ensure consistent solvent throughout, 600 µL of ethanol was added to solutions without TMB then made up to 2 mL with PBS (pH = 5.0), since TMB solution is made in ethanol. The solutions were incubated for 50 mins with 800 rpm shaking in dark conditions, after which they were centrifuged and supernatant absorbance measured, as usual. Samples were run in triplicates for average and standard deviation calculations, represented by error bars.

2.6.2 H_2O_2 Radical Production by Fe-BTC

To identify the type of H_2O_2 radical produced by the peroxidase activity of Fe-BTC, tert-butyl alcohol, an $OH^{\cdot}$ radical scavenger [12], was added at different volumes to the Fe-BTC-TMB-

H_2O_2 biosensor system. Specifically, solutions with varying tert-butyl alcohol volumes ranging from 0 to 500 µL were prepared as follows. 0.75 mg/mL Fe-BTC (375 µL of 4 mg/mL stock Fe-BTC solution), TMB at 3 mM (600 µL of 10 mM TMB stock solution in ethanol), and 100 µM H_2O_2 (40 µL of 1 mM stock). Then, different volumes of tert-butyl alcohol were added to the vials and made up to 2 mL with PBS (pH 5.0). The procedure was continued as per the LOD experiment protocol (Section 2.4).

2.6.3 Fe-BTC Adsorption Behaviour

MOFs demonstrate high adsorption capacities and are used extensively in dye removal applications [21–23]. As H_2O_2 detection with Fe-BTC relies on using TMB dye, the tendency of Fe-BTC to adsorb TMB and the subsequent impact on H_2O_2 detection were investigated. Samples were prepared by adding 375 µL of 4 mg/mL Fe-BTC and 600 µL of 10 mM TMB in Eppendorf vials and at two H_2O_2 concentrations: 40 µM (low) and 150 µM (high), where 200 µL (30 µL) of 400 µM (10 mM) H_2O_2 stock was added to prepare 40 µM (150 µM) H_2O_2 samples. Finally, all samples were made up to 2 mL with pH = 5.0 PBS. Two preparation methods were tested to understand adsorption: the first method involved mixing Fe-BTC, TMB, and H_2O_2 all together directly while the other one involved mixing Fe-BTC with TMB first and incubating for 30 mins, followed by adding H_2O_2. 30 mins incubation time was chosen based on previous studies on Fe-BTC applications in dye adsorption, where rapid dye adsorption is seen in the first 30 –180 mins [24]. Both sets were then incubated for 50 mins at 800 rpm in the dark, then centrifuged at 12000 rpm for 5 mins. The supernatant was collected, and the TMB absorption spectra were determined using a UV-Vis spectrophotometer at the characteristic TMB oxidation peak of 660 nm, with absorbance measured from 400 nm to 800 nm. Triplicate samples were run for average and standard deviation calculations, represented by error bars.

2.8 Cholesterol LOD Determination using Fe-BTC

Cholesterol detection by the Fe-BTC system requires first incubating cholesterol in ChOx for a specific period, to produce H_2O_2. The ChOx–cholesterol incubation parameters investigated include incubation time and ChOx concentration. Meanwhile, the pH of PBS solution was maintained at 7.4 for all samples, as this pH has been previously identified as the optimal pH reported for ChOx activity [14,25]. Two ChOx-cholesterol incubation temperatures were tested: room temperature (25 ºC), which is favored for less energy consumption, and physiologic temperature (37 ºC), which is the optimal temperature for enzyme function [14,25]. After incubation, Fe-BTC, TMB, and PBS (pH = 5.0) are added to the mixture to react with the produced H_2O_2, which subsequently oxidizes TMB to produce a color change. This procedure follows the previously established protocol for H_2O_2 detection, enabling the determination of ChOx–cholesterol incubation conditions for improved cholesterol sensing performance. The full, two-step protocol used for cholesterol parametric studies and LOD studies is illustrated in Figure 3. As illustrated, the first step involves ChOx-cholesterol incubation in PBS (pH = 7.4) for 30 mins at 25 or 37 ºC. Then, the second stage involves adding Fe-BTC, TMB, and PBS (pH = 5.0) with shaking in the dark at 25 ºC for 50 mins, followed by centrifugation. Then, the supernatant is collected for absorbance measurements.

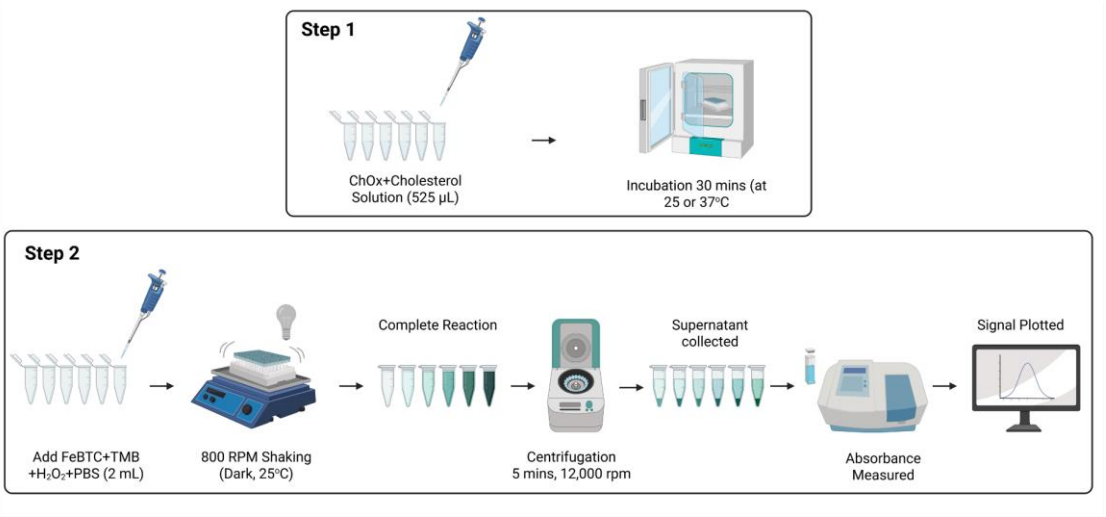

Figure 3: General experimental protocol for cholesterol parametric and LOD studies.

To determine the limit of detection of the proposed Fe-BTC biosensor system, different cholesterol concentrations were incubated with ChOx, then reacted with Fe-BTC and TMB to produce a color change. Absorbance measurements were used to quantify the resulting color change and determine cholesterol concentration. 250 µM cholesterol stock was used to prepare solutions with low cholesterol concentrations (0.0 – 100.0 µM in 525 µL, equivalent to 0.0 – 26.25 µM in 2 mL) while 1500 µM cholesterol stock solution was used for preparing high cholesterol concentrations (150.0 – 400 µM in 525 µL, equivalent to 39.375 – 105.0 µM in 2mL). It is important to note that the ideal ChOx concentration for both 25 ºC and 37 ºC incubation was determined to be 0.5 mM in 525 µL (= 131.25 µM in 2 mL final solution). However, LOD experiments using room temperature (RT, 25 ºC) ChOx-incubation were performed using 1.5 mM ChOx in 525 µL. Experiments were conducted using a single concentration to evaluate the system feasibility, while future studies will explore the effect of optimized enzyme concentrations on cholesterol detection in greater detail. min.

For experiments with ChOx–cholesterol incubation at room temperature, 1.5 mM ChOx (225 µL of 3.5 mg/mL ChOx stock) were added to Eppendorf vials. Then, the solution was made up to 525 µL with varying cholesterol concentrations (0 – 400 µM) and PBS (pH = 7.4). Meanwhile, for experiments with ChOx–cholesterol incubation at 37 ºC, 0.5 mM ChOx (75 µL of 3.5 mg/mL ChOx stock) was used instead. For both 25 ºC and 37 ºC samples, solutions were left to incubate for 30 minutes. Then, TMB at 3 mM (600 µL of 10 mM TMB stock solution in ethanol), 0.75 mg/mL Fe-BTC (375 µL of 4 mg/mL stock Fe-BTC solution) and 500 µL of PBS (pH = 5.0) were added to each Eppendorf vial, to dilute all samples to 2 mL. The solutions were incubated for 50 mins with 800 rpm shaking in dark conditions, after which they were centrifuged at 12000 rpm for 5 mins. The supernatant was collected, and the TMB concentrations were determined using a UV-Vis spectrophotometer at 660 nm, with absorbance measured from 350 nm to 800 nm. Triplicate solutions were made for each cholesterol concentration tested at each temperature, for average and standard deviation calculations, represented by error bars. Figure 3 illustrates the general experimental protocol followed. A plot of absorbance against cholesterol concentration (after dilution) is generated, and the limit of detection (LOD) is calculated according to Equation (1).

2.9 Selectivity Studies

The selectivity of the Fe-BTC-based biosensor to H_2O_2 and cholesterol was determined by testing H_2O_2 and cholesterol detection, separately, in the presence of interfering analytes generally present in blood serum samples. The experimental methods adopted match the optimized methods previously described. The selectivity of the Fe-BTC-based biosensor in detecting 20 μM H_2O_2 was tested in the presence of glycine, L-lysine, L-cysteine, uric acid, urea, glucose, sucrose, fructose, NaCl, KCl, $CaCl_2$, and a mixture of all, with and without L-cysteine, at 20 μM, and NaCl at 200 μM to mimic blood levels. Meanwhile, the selectivity of Fe-BTC-based biosensor in detecting ~ 40 μM cholesterol (in 2 mL) was tested in the presence of L-cysteine, uric acid, glucose, fructose, NaCl, and a mixture of all, with and without L-cysteine, at equal concentration. NaCl was also tested at ~ 400 μM, to mimic blood concentrations where NaCl is generally over 10x higher than cholesterol levels [26]. ChOx-cholesterol incubation was performed at 37 ºC, following the operating conditions described above. All samples were run in triplicates for average and standard deviation calculations, represented in error bars. Statistical analyses were performed using Origin Pro. A paired sample t-test was conducted to evaluate significant differences between two related groups. Paired plots were generated to visually represent the relationship between paired observations, with each line connecting data from the same sample under different conditions. Results were considered statistically significant at $p < 0.001$.

3. Results and Discussion

3.1 Characterization

Fe-BTC, the peroxidase mimic used to facilitate cholesterol and H_2O_2 detection, was characterized using FT-IR, XRD, SEM, EDS mapping, XPS, and zeta potential. FT-IR analysis provides information regarding the chemical bonds and groups present in Fe-BTC, which provides insights into the peroxidase behaviour of Fe-BTC. The FT-IR spectrum of Fe-BTC is shown in Figure 4(a). The spectrum resembles Fe-BTC FTIR spectra reported in the literature [27,28]. The broad absorption band at 3400 – 3650 cm^{-1} is attributed to O-H bond, likely due to water adsorption in Fe-BTC pores. Meanwhile, the bands at 1629 and 1573 cm^{-1} and 1450 and 1375 cm^{-1} are attributed to the symmetric and asymmetric stretching of C=O group in 1,3,5-benzenetricarboxylic acid (BTC) ligand carboxylate group, respectively [27,28]. Carboxylic C-O stretching is also confirmed by the weak peak at 1109 cm^{-1}. Finally, peaks at 761 and 712 cm^{-1} represent C-H bond bending, while the Fe-O bond, confirming Fe complexation to BTC ligand, is confirmed by the peak at 600 cm^{-1}. The presence of Fe(III) centers plays a major role in the peroxidase activity of Fe-BTC, similar to iron centers present in the enzyme HRP [29,30]. Overall, the FT-IR spectrum matches the reported literature [27,28] and confirms the presence of main chemical groups in Fe-BTC: Fe centers and BTC ligand.

The XRD spectrum of Fe-BTC is shown in Figure 4(b). The spectrum indicates the amorphous nature of Fe-BTC, due to the presence of broad peaks. However, some crystalline regions are observed, indicated by the peak at 2θ = 10-12º. The XRD spectrum obtained is mostly comparable with the literature, which also reported the amorphous nature of Fe-BTC with little crystallinity [31–34]. Furthermore, SEM images of Fe-BTC at 1 μm magnification is shown in Figure 4(c). The morphology of Fe-BTC appears to be irregular, where small, round-like aggregates and clusters are observed. This is common for amorphous MOFs and is similar to SEM images reported in the literature of Fe-BTC [33,35]. This amorphous, irregular nature

may offer greater exposed surface areas as active sites for peroxidase activity and more rapid, sensitive detection [17].

Zeta potential is an important characterization techniques to determine the surface charge of MOFs and their stability in suspensions [36–39]. The results of the zeta potential analysis is shown in Figure 4(d). Average Fe-BTC zeta potential, measured in distilled water at pH = 7.4, was found to be -15.83 mV. Generally, higher absolute zeta potential values indicate greater suspension stability due to strong repulsion between nanoparticles, while absolute zeta potential values ranging from 0 -10 mV have low suspension stability [36]. Fe-BTC zeta potential of -15.83 indicates moderate stability in suspension, with potential to aggregate over time, similar to reported literature [36,40]. It is important to note that zeta potential was measured in distilled water, while cholesterol biosensing is performed with Fe-BTC suspended in PBS at pH 5.0. A study found the zeta potential of Fe-BTC suspended in DW at pH 5.0 also ~15 mV, confirming moderate stability [40]. Further characterization studies of Fe-BTC's zeta potential in PBS can be considered to better reflect the actual biosensor medium.

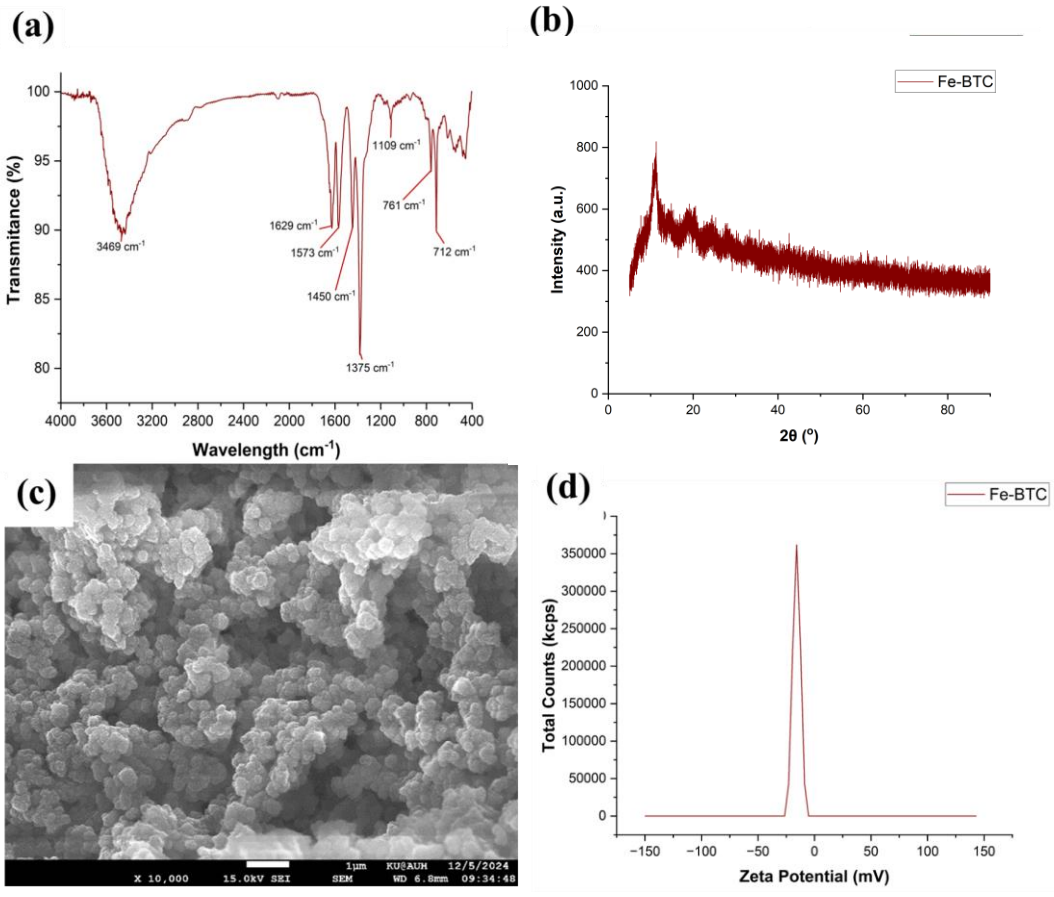

Figure 4: Fe-BTC characterization tests: (a) FT-IR spectrum, (b) XRD of Fe-BTC, (c) SEM image of Fe-BTC at 1 µm magnification and (d) Average Zeta Potential Measurements

EDS allows for bulk elemental analysis of Fe-BTC to quantify elements present. The EDS spectrum of Fe-BTC and the elemental mapping are shown in Figure 5, with the insert revealing the weight percentage of each element present. The EDS spectrum matches that reported in the literature [41]. The high weight percentage of iron (31.2 %) may be correlated to high

peroxidase activity, since iron plays the major role in peroxidase reactions [29,30]. The EDS color maps shown in Figure 5 also reveal the regular distribution of the elements on Fe-BTC surface.

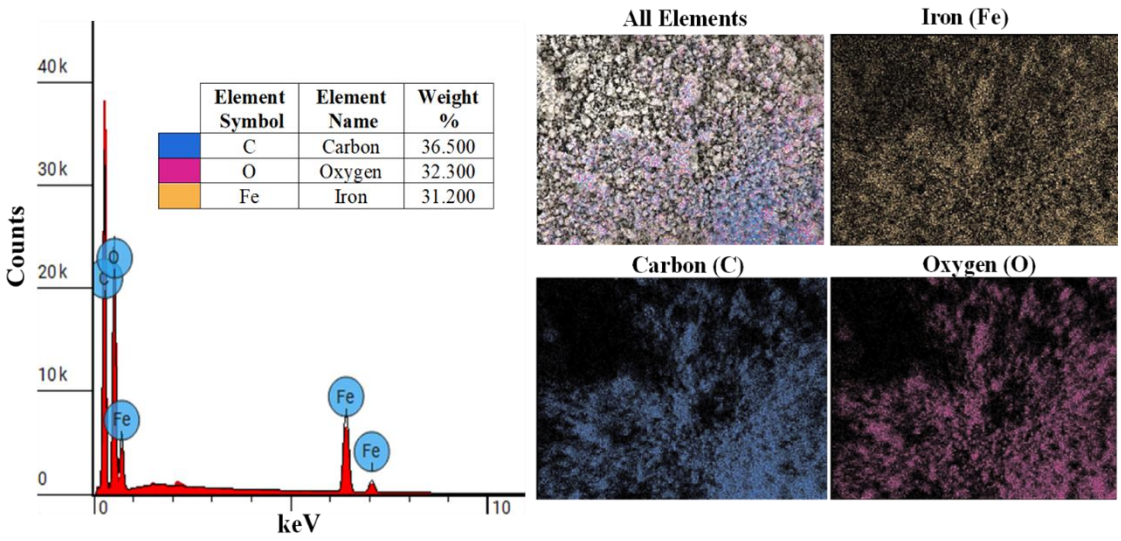

Figure 5: EDS color map of Fe-BTC, displaying the distribution of carbon, oxygen, and iron atoms in Fe-BTC sample.

XPS analysis, like EDS, facilitates elemental analysis of Fe-BTC; however, XPS analysis focuses on surface elemental composition [42]. The XPS spectra of all elements and individual Fe, C, and O are illustrated in Figure 6 (a-d). As can be seen, the results agree with EDS results, revealing the presence of three main elements: iron, carbon, and oxygen. Furthermore, trace amounts of nitrogen were also detected, as shown in the spectrum at binding energy ~400 eV, which may be attributed to slight contamination. Finally, peaks in the C 1 spectrum represent different hybridization states of carbon in Fe-BTC, related to C-C, C=C, and C=O bonds [43]. More specifically, the peak at 285 eV is representative of the aromatic ring in Fe-BTC, while the peak at 289 eV represents the carboxyl group in Fe-BTC, as highlighted in Figure 6(d). The The Fe 2p deconvolution results are presented and discussed in the supplementary document (Figure S1).

Overall, the results are in agreement with published literature [44] and with FT-IR and EDS analyses discussed.

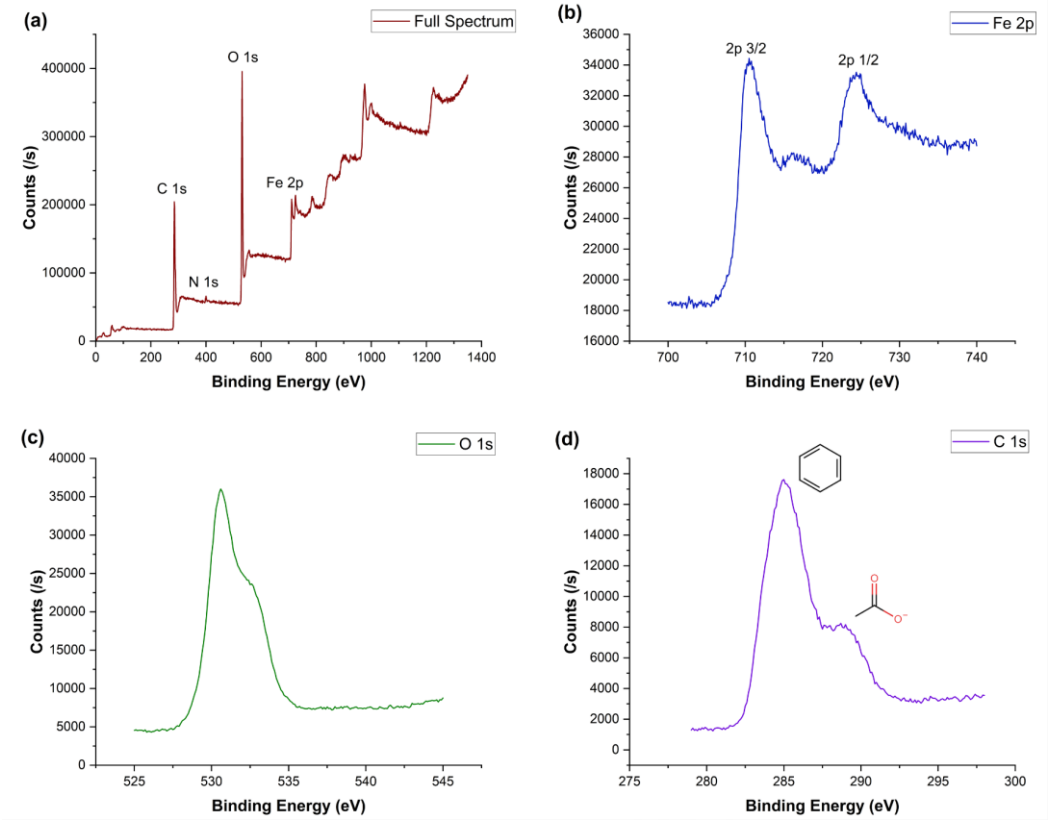

Figure 6: XPS results: (a) Full (b) Fe 2p, (c) O 1s, and (d) C 1s Spectra of Fe-BTC.

3.2 H_2O_2 Detection by Fe-BTC-based Sensor

Parametric studies were conducted first to determine the best pH, time, TMB concentration, and Fe-BTC concentrations for H_2O_2 detection. pH was varied from 5.0 – 8.0. As shown in Figure 7(a), the intensity of absorbance decreases with increasing pH up to a value of 7.4, after which the curve plateaus and no absorbance is observed. This indicates that better colorimetric responses from TMB are obtained in acidic conditions. Thus, pH was set to 5.0 for further experiments, given the darkest color observed at that pH level. Similarly, the absorbance intensities at different time points over 60 mins are shown in Figure 7(b). The colorimetric response increases up to 20 mins, after which the reaction seems to stabilize for 20 mins. Then, the reaction continues and a sharp in absorbance is observed at 50 mins, after which a plateau is obtained, indicating a complete reaction. The absorbance intensities of the color changes obtained with varying TMB concentrations are depicted in Figure 7(c). Furthermore, the intensity of the color change increases up to TMB concentration of 3.0 mM, after which the intensity decreases. A change in the color from blue to green is noticed at higher TMB concentrations, attributed to the presence of yellow TMB, due to complete oxidation [45]. Finally, the absorbance intensities of the color changes obtained with varying Fe-BTC concentrations are illustrated in Figure 7(d). The intensity of the color change increases up to Fe-BTC concentration of 0.75 mM, after which the intensity decreases significantly. This decrease may be attributed to the adsorption of the dye into the excess Fe-BTC active sites. The small standard deviation ranges indicate the high repeatability of the data. Hence, pH 5.0, 50 mins incubation time, 3 mM TMB concentration, and 0.75 mg/mL Fe-BTC were chosen as the operating parameters used for subsequent experiments, due to the maximum response obtained at these points.

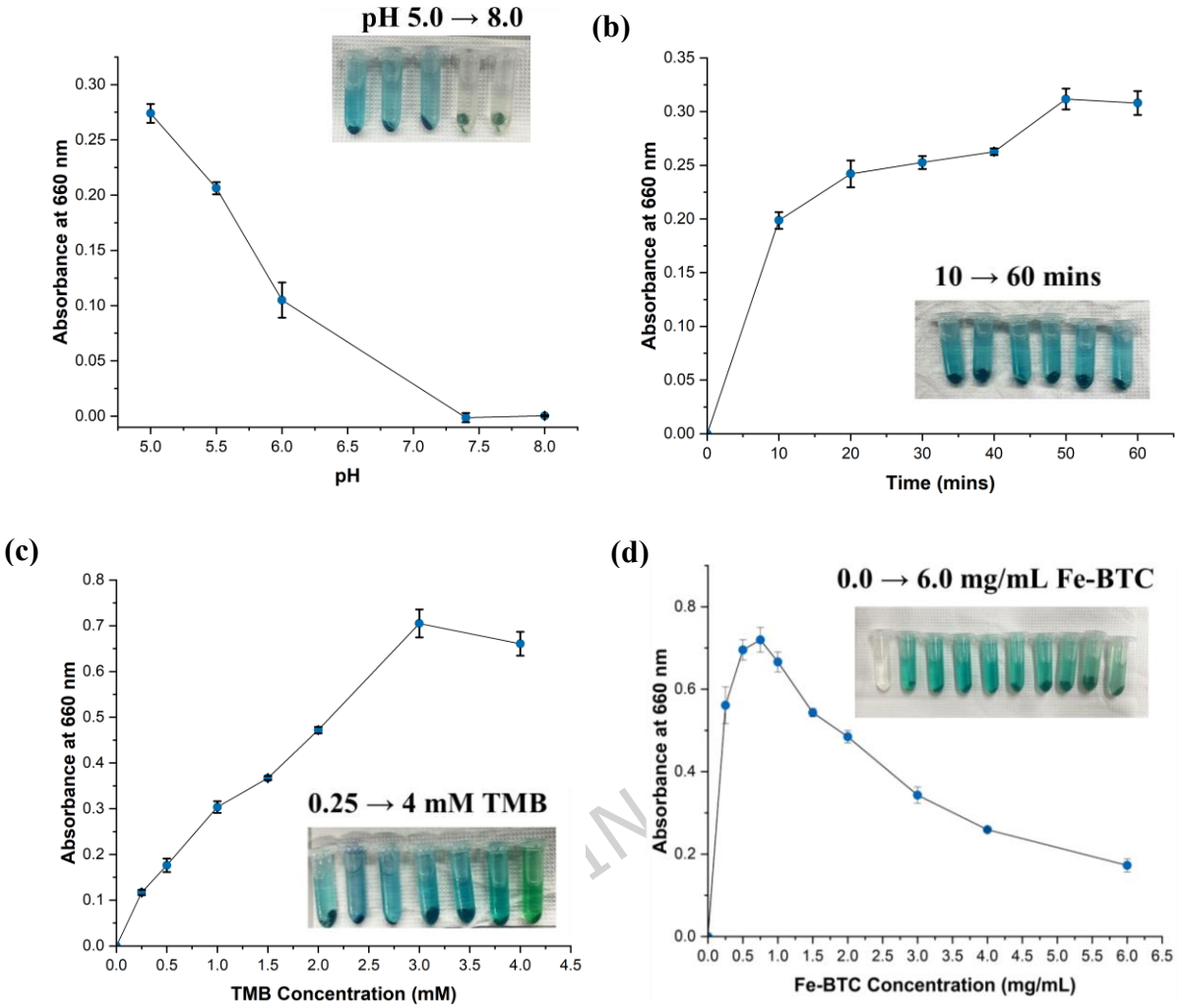

Figure 7: H_2O_2 parametric studies: (a) pH optimization for H_2O_2 detection using 0.5 mg/mL Fe-BTC, 1 mM TMB, 500 µM H_2O_2, and 30 mins incubation time, (b) incubation time optimization for H_2O_2 detection, using 0.5 mg/mL Fe-BTC, 1 mM TMB, 500 µM H_2O_2, and PBS (pH 5.0), (c) TMB concentration optimization for H_2O_2 detection, using 0.5 mg/mL Fe-BTC, 500 µM H_2O_2, PBS (pH 5.0) and 50 mins incubation time, (d) Fe-BTC concentration optimization for H_2O_2 detection, using 3 mM TMB, 500 µM H_2O_2, PBS (pH 5.0) and 50 mins incubation time. Error bars represent the standard deviations of three trials. Inserts show the change in color intensity.

Detection of H_2O_2 concentrations from 0 µM to 1000 µM by Fe-BTC-TMB system was investigated at the chosen, optimal conditions: using PBS at pH 5.0, incubation for 50 mins, TMB concentration of 3.00 mM, and Fe-BTC concentration of 0.75 mg/mL. The absorbance intensities obtained at each H_2O_2 concentration tested are shown in Figure 8. The results demonstrate good sensitivity and excellent linearity (R^2 ~0.99) for the three linear detection regions: 0 – 100 µM, 100 – 267 µM, and 267 – 800 µM. The calibration curve exhibits three distinct linear regions, which can be attributed to changes in catalytic kinetics and substrate availability. At low H_2O_2 concentrations, the reaction rate increases proportionally with substrate concentration, while in the intermediate region, partial occupation of Fe-BTC active sites leads to a slower response. At higher concentrations, the system approaches catalytic saturation, resulting in a more reduced slope [18,46].

The highest sensitivity of 0.0028 is observed at the first linear region with a LOD of 3.30 µM, which is lower than the LOD obtained using a Bimetallic Eu/Fe-MOF (LOD = 5.0 µM) [19]. The obtained LOD is also comparable to relevant MOFs reported in the literature with LODs ranging from 1 – 5 µM [14,18,47]. Moreover, recent studies demonstrated low LODs in the nanomolar ranges; however, many of these sensors were complex, hybrid MOF systems and/or operated at high temperatures and at longer detection time, which can limit their use in point of care (PoC) devices for real applications (see Table S1). Meanwhile, the proposed biosensor operates at room temperature, which makes it easier to use in PoC devices. Moreover, normal blood cholesterol concentrations generally lie in high micromolar ranges and do not exceed 5200 µM [48]. Thus, when reacted with ChOx, high micromolar concentrations of H_2O_2 will be produced, which can be detected by the proposed system directly or after sample dilution. Thus, the LOD obtained by the present sensing platform is still comparable to previous similar sensing systems and remains acceptable and applicable for blood cholesterol detection. Thus, the Fe-BTC-TMB system is successful for detecting H_2O_2 from 5 – 800 µM, with an LOD of 3.30 µM.

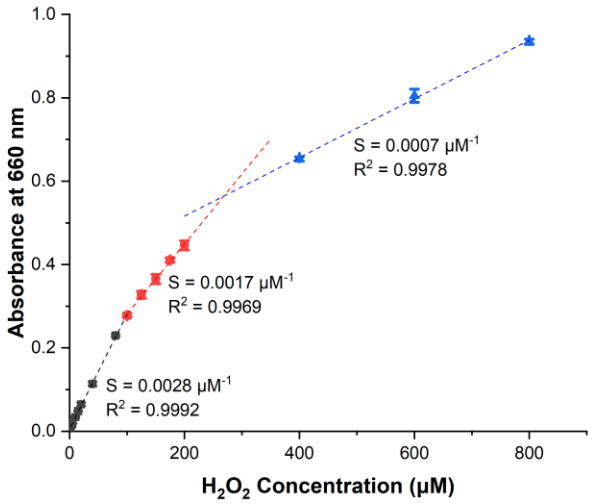

Figure 8: Calibration curve for H_2O_2 detection by Fe-BTC-TMB system, using 0.75 mg/mL Fe-BTC, 3 mM TMB, PBS (pH 5.0), and 50 mins incubation time. Error bars represent the standard deviations of three trials. Dashed lines correspond to a linear fit. Insert shows the change in color intensity at 0.0– 800.0 µM H_2O_2.

3.3 Fe-BTC Peroxidase Activity and H_2O_2 Detection Mechanism

The peroxidase activity of Fe-BTC is the key catalytic reaction responsible for TMB oxidation and H_2O_2 detection. To confirm this sensing mechanism, a series of experiments were conducted to characterize Fe-BTC peroxidase activity and H_2O_2 radical formation. Furthermore, the impact of the adsorptive nature of Fe-BTC in the presence of TMB was analyzed.

3.3.1 Peroxidase System Components and Interactions

To understand the peroxidase activity of Fe-BTC and mechanism of H_2O_2 detection by Fe-BTC-TMB system, the UV-Vis absorbance spectra of the individual system components (Fe-BTC, TMB, H_2O_2, PBS), different combinations (Fe-BTC+H_2O_2, Fe-BTC+TMB, TMB+H_2O_2), and full biosensor system (Fe-BTC+TMB+H_2O_2) were recorded at wavelength range of 350 – 800 nm. These absorbance spectra are illustrated in Figure 9. As shown, all combinations and individual components have no significant absorbance. Indeed, only the full FeBTC+TMB+H_2O_2 system demonstrates significant TMB oxidation and blue color change, conveyed by a major peak at 660 nm. The inserted photograph of the samples further proves this, where only the final, complete biosensor system demonstrates a dark blue color. All other samples are colorless. This is similar to the results obtained by other peroxidase-like nanomaterials, where removing the peroxidase-mimic leads to no color change and thus no H_2O_2 detection [12,49]. For the Fe-BTC-TMB sample, a very minor peak is observed and a slight color change, suggesting minor oxidase-like activity of Fe-BTC since some TMB was oxidized despite the absence of H_2O_2. However, this effect is minor. This was also observed in a hybrid Au/CeO_2 nanorod-CuMOF-based biosensor system, but with greater oxidase effect and higher signal [49]. Thus, Fe-BTC peroxidase activity is mainly responsible for catalysis of H_2O_2 reduction and TMB oxidation, for the resultant blue color change.

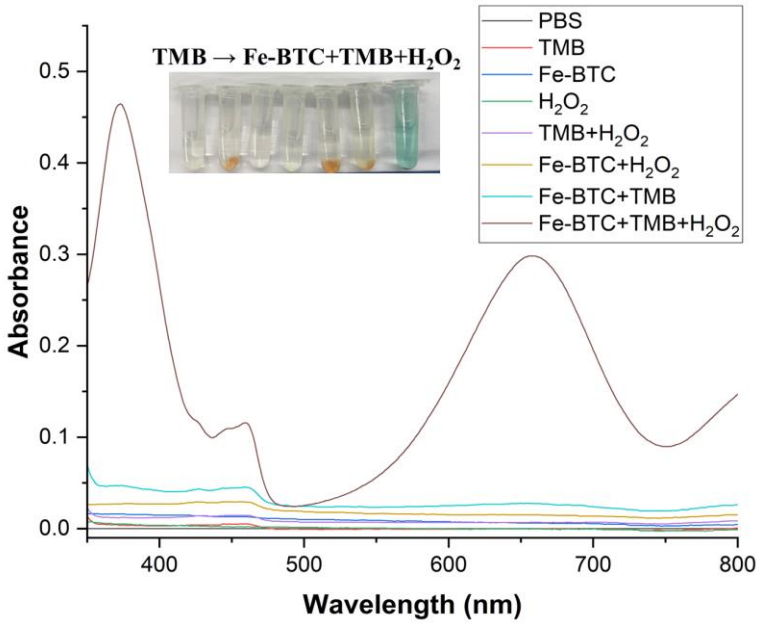

Figure 9: Average absorbance spectra of Fe-BTC-TMB-H_2O_2 system components. Insert shows color change of samples PBS to Fe-BTC+TMB+H_2O_2, in the same order as the legend.

3.3.2 H_2O_2 Radical Production by Fe-BTC

Nanomaterials with peroxidase-like activity, called nanozymes, are proposed to decompose H_2O_2 into OH· radicals, which in turn oxidize TMB. In Fe-based nanomaterials, H_2O_2 decomposition is intermediated by Fe^{2+} ions, which react with H_2O_2 in a redox reaction to produce OH·, which undergoes further reduction to water [30]. The chemical reaction is shown in Equations (2)-(4) below.

$$Fe^{2+} + H_2O_2 \rightarrow Fe^{3+} + OH^- + OH\cdot \quad (2)$$

$$OH\cdot + e^- \rightarrow OH^- \quad (3)$$

$$OH^- + H^+ \rightleftharpoons H_2O \quad (4)$$

To confirm that Fe-BTC follows this mechanism, tert-butyl alcohol, an OH· radical scavenger, is added at different volumes to the Fe-BTC-TMB-H_2O_2 system. If OH· radicals are present, t-butyl alcohol would compete with TMB to react with OH·, thus less TMB would be oxidized and reduced color intensity would be observed. The results of adding tert-butyl alcohol to the biosensor system is illustrated in Figure 10. Clearly, the absorption at 660 nm, attributed to blue oxTMB, decreases significantly with increasing tert-butyl alcohol volumes, as shown in the full spectrum (Figure 10 (a)) and the plot of average absorbance at 660 nm (Figure 10(b)). The insert picture of the samples further confirms reduced TMB oxidation, as the samples become less blue and more yellow with increasing tert-butyl alcohol volumes. Hence, Fe-BTC peroxidase is confirmed to reduce H_2O_2 via OH· radical formation, and OH· radicals are the major active intermediates in TMB oxidation. This was observed in a similar MOF-based system, using Fe_3O_4@MIL-100(Fe) [12].

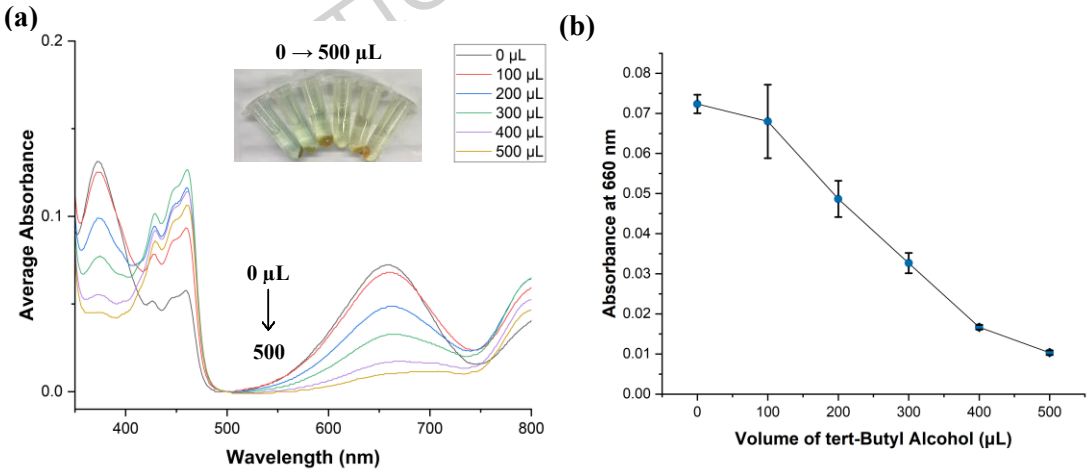

Figure 10: H_2O_2 Radical Production by Fe-BTC: (a) Average absorption spectra of Fe-BTC-TMB-H_2O_2 system with addition of tert-butyl alcohol at different volumes and (b) absorption at 660 nm. Error bars represent the standard deviations of three trials. Insert shows the change in color intensity with addition of 0 – 500 µL tert-butyl alcohol.

3.3.3 Fe-BTC Adsorption Behaviour

Fe-based MOFs, and Fe-BTC specifically, demonstrate high adsorption capability, and have been reported for use in dye removal applications [21–23]. However, in our biosensor, Fe-BTC's adsorption of TMB dye may reduce the sensing performance by adsorbing TMB dye, thereby reducing the amount of TMB available for oxidation and thus reducing observed color change. The method of mixing biosensor reagents and time taken may impact TMB adsorption by Fe-BTC. To test this, Fe-BTC-TMB-H_2O_2 biosensing system was prepared via two methods. The first method, which is the method followed throughout, involves mixing all reagents together within a short time frame then incubating for 50 mins with 800 rpm shaking in the dark as usual. The second method involves mixing Fe-BTC an TMB together first and allowing them to incubate for 30 minutes without shaking. Then, H_2O_2 is added, and the reaction is incubated in the dark at 800 rpm for 50 mins. This was tested with two H_2O_2 concentrations: 40 µM and 150 µM.

The absorbance value at 660 nm of the biosensor systems prepared by both methods is shown in Figure 11. At high H_2O_2 concentration, incubation of Fe-BTC and TMB together first led to significant adsorption of TMB, which resulted in less TMB availability and lower absorbance at 660 nm by biosensor. Meanwhile, no significant change in absorbance was observed at 40 µM H_2O_2, which can be attributed to the availability of enough free TMB (not adsorbed) for oxidation by lower H_2O_2 concentrations. Hence, it is best to mix all reagents together directly when preparing Fe-BTC-TMB-H_2O_2 biosensor, to minimize adsorption effects. This is useful when designing PoC devices, where reagents should be supplied to users separately rather than being mixed and packaged together, to reduce adsorption.

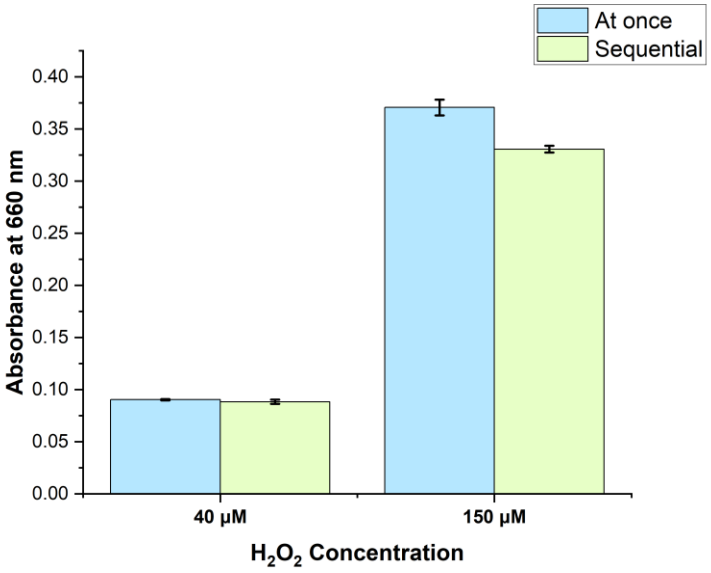

Figure 11: Bar chart of absorption of Fe-BTC-TMB-H_2O_2 system at 40 µM and 150 µM using two preparation methods: mixing all components together [at once] or mixing of Fe-BTC and TMB first for 30 mins, then adding H_2O_2 [sequential].

3.4 Cholesterol Detection by Fe-BTC-based Sensor

The operating conditions of time and ChOx concentration for cholesterol detection were selected by parametric studies. ChOx-cholesterol incubation time was varied from 0 to 60 minutes. The

absorbance intensities of the color changes obtained with ChOx-cholesterol incubation times are illustrated in Figure 12(a). The absorbance intensity of the color change increases slightly with increasing time from 0 to 60 mins; however, the increase is not significant. The insert, displaying the actual samples, also shows a minor color change with each incubation time. Furthermore, varying the incubation temperature from 25 ºC to 37 ºC had no significant effect on incubation time effects. The lack of significant impacts of cholesterol-ChOx incubation times may be attributed to the second reaction step involving further incubation for 50 mins. ChOx may continue reacting with cholesterol to completion during the second incubation period, despite the presence of Fe-BTC and TMB and the change in pH (5.0). Future studies may look into mixing all reagents together, excluding separate incubation of ChOx with cholesterol. For LOD experiments, 30 mins was chosen as the ChOx-cholesterol incubation time for both 25 ºC and 37 ºC incubation, to ensure complete reaction.

The absorbance intensities of the color changes obtained with increasing ChOx concentration are illustrated in Figure 12(b). The absorbance intensity of the color change increases when the ChOx concentration increases to 131.25 µM (final concentration in 2 mL), after which the absorbance decreases with increasing ChOx concentrations. The inserted picture of the samples illustrates the initial decrease in color intensity up to 131.25 µM ChOx concentrations, after which the color intensity decreases with increasing ChOx concentrations. Again, varying the incubation temperature from 25 ºC to 37 ºC showed similar trends, with no impact on ChOx activity. However, 25 ºC incubation resulted in higher absorbance and deeper color intensity, compared to 37 ºC. Thus, the best ChOx concentration for both 25 ºC and 37 ºC ChOx-cholesterol incubation is 0.5 mM (in 525 µL), equivalent to 131.25 µM after addition of all biosensor reagents and dilution to a final volume of 2 mL.

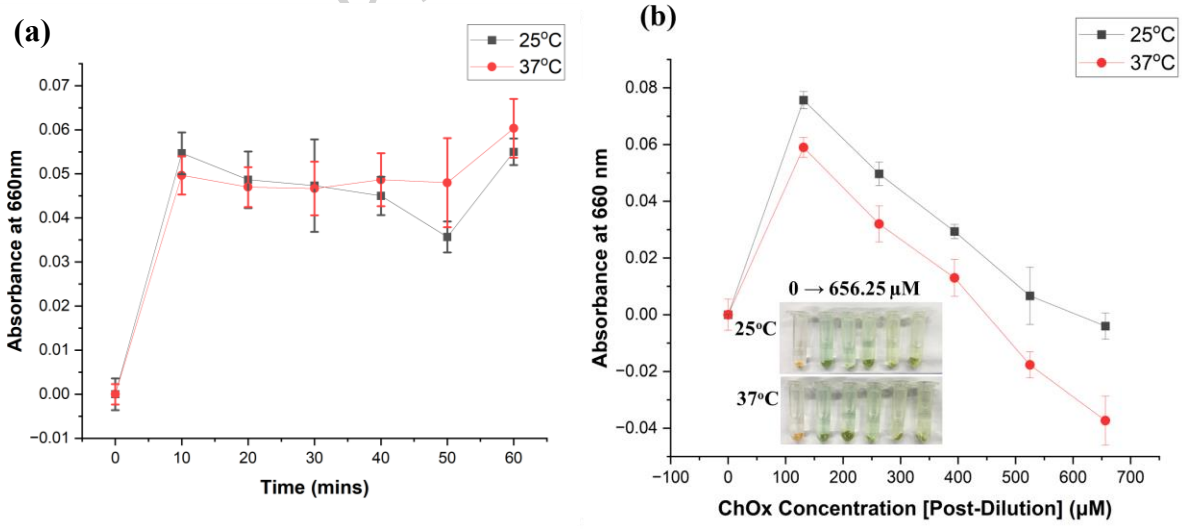

Figure 12: ChOx-Cholesterol parametric studies: (a) ChOx-Cholesterol incubation time and (b) ChOx concentration parametric studies for cholesterol detection at ChOx-cholesterol incubation temperatures of 25 ºC and 37ºC. Error bars represent the standard deviations of three trials. Insert shows the change in color intensity at 25 ºC and 37ºC at each point.

Parametric studies of ChOx-cholesterol incubation time and ChOx concentration concentrations revealed that the overall optimum conditions for cholesterol detection when incubating at room temperature (25 ºC) or 37 ºC was 0.5 mM ChOx (in 525 µL; equivalent to 131.25 µM in 2 mL final solution) and 30 mins incubation time. Incubation temperature had no major impact on optimal cholesterol detection conditions by the Fe-BTC-TMB system when varied between RT and 37 ºC.

Detection of cholesterol concentrations from 0 µM to 105 µM by the Fe-BTC-TMB system was investigated using two ChOx-cholesterol incubation temperatures: 25 ºC and 37 ºC. The absorbance intensities obtained at each cholesterol concentration tested with RT and 37 ºC ChOx-cholesterol incubation are shown in Figure 13 and Figure 14, respectively. The absorbance intensity at 660 nm increases linearly with increasing cholesterol concentration, as demonstrated by the darkening color of samples (shown in the insert of Figures 13 and 14). The LOD obtained at RT and 37 ºC ChOx-cholesterol incubation are 2.91 µM and 2.88 µM, respectively, with a linear cholesterol detection range of 6.56 – 78.75 µM for both tested operating temperatures. Thus, the ChOx-FeBTC-TMB system is robust and temperature independent, allowing for minimal energy usage by achieving similar results at lower incubation temperatures. The LOD determination at room temperature for ChOx-cholesterol incubation was conducted using a ChOx concentration of 393.75 µM. Future studies can explore further improvement of the biosensing system, along with evaluating the impact of reduced ChOx-cholesterol incubation times or implementing a streamlined one-step reaction by combining all reagents, as an alternative to the current two-step process.

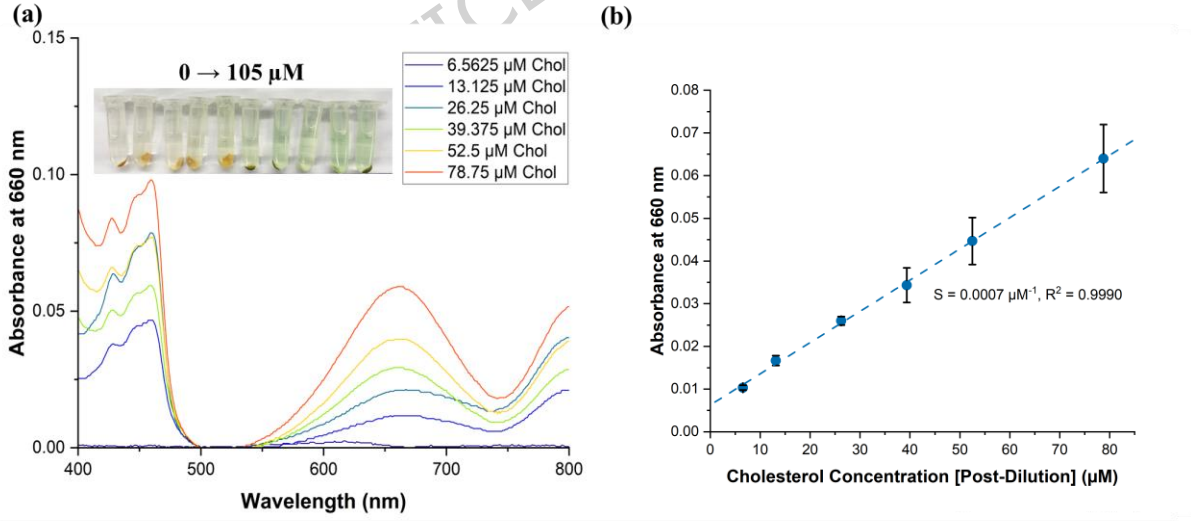

Figure 13: Cholesterol LOD determination at 25ºC: (a) Average absorption spectrum and (b) LOD calibration curve for cholesterol detection by Fe-BTC-TMB-ChOx Biosensor system at RT ChOx-cholesterol incubation. Error bars represent the standard deviations of three trials. The dashed line represents a linear fit. The insert shows the change in color intensity at 0.0– 105 µM cholesterol.

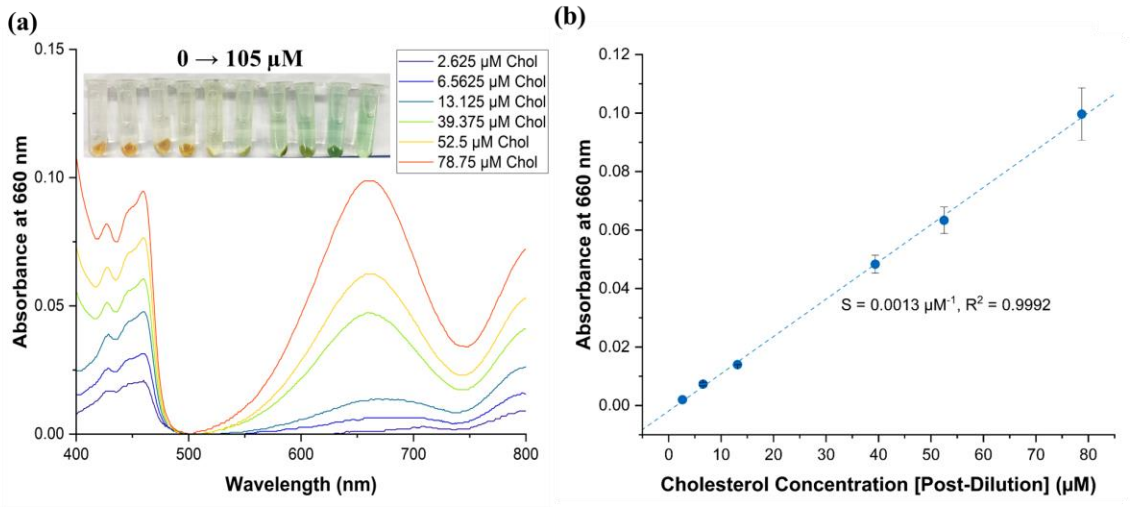

Figure 14: Cholesterol LOD determination at 37 ºC: Average absorption spectrum and LOD calibration curve for cholesterol detection by Fe-BTC-TMB-ChOx Biosensor system at 37 ºC ChOx-cholesterol incubation: (a) absorption spectra averaged over three trials and (b) calibration curve for determining limit of detection (LOD). Error bars represent the standard deviations of three trials. The dashed line represents a linear fit. The insert shows the change in color intensity at 0.0 – 105 µM cholesterol.

The cholesterol LOD values obtained are comparable to many relevant MOFs reported in the literature [18,19,47,50]. For example, MIL-101(Fe) functionalized with bifunctional carbon quantum dots (CQDs) demonstrated effective cholesterol detection with an LOD of 4.55 µM [18], which is slightly greater than the LOD achieved in this study. Meanwhile, LODs of 1.57 µM and 1.2 µM were achieved by hyrbid MnO_2 nanosheets functionalized on Tb-MOFs and Mo-doped Cu-2MI MOF sensors, respectively [47,50]. However, other studies reported significantly lower LODs in the nanomolar ranges, as shown in Table S2. These studies adopted different approaches, with MOFs used for ChOx and/or HRP immobilization [51,52], MOFs used as nanozymes peroxidase mimics [12,13], and MOFs used for direct, enzyme-free cholesterol detection [53,54]. Colorimetric, fluorescent, and chemiluminescent detection techniques were used, achieving LOD values ranging from nanomolar to millimolar concentrations (see Table S2). The major MOF-based sensing mechanism employed involved colorimetric detection using MOFs as peroxidase nanozymes, similar to the work proposed in this research. However, many peroxidase-mimics adopted hybrid nanomaterials, combining MOFs with other nanoparticles, which impose the use of complex synthesis protocols and expensive materials [12–14,18,47,49,55]. Examples of hybrid MOF-based sensors reported include Pd nanoclusters in ZIF-8 [14], Co_3O_4@CuMOF nanoparticles [55], and UiO-66 functioalized with graphene quantum dots (GQDs/UiO-66) [13], among any others (see Table S2). Furthermore, many report narrow linear ranges, which require careful dilution of blood samples for real applications [11,56,57]. Only a few used pure MOF as nanozymes [11,19], with only MIL-101(Cr) available commercially on a large scale [11,58]. Hence, an additional advantage of our Fe-BTC-based biosensor is its simplicity, with no complex hybrid system, and its high availability commercially, allowing for easier adaptation in PoC devices.

Notably, some of the studies in Table S2 adopted higher operating temperatures and longer detection time, which can reduce the LOD but also limit real applications in PoC devices.

Meanwhile, our biosensor shows excellent operation at room temperature, which is easier to use in PoC devices. Moreover, normal blood cholesterol concentrations generally lie in high micromolar ranges and do not exceed 5200 μM [48]. As such, our biosensor can easily detect cholesterol in blood after its dilution while operating in the linear range. Hence, the LOD obtained by the present sensor, although higher than some reported in the literature, is comparable to many other studies and remains acceptable and applicable for blood cholesterol detection. In addition, the sensing system's simple, pure make-up (only Fe-BTC with no hybrid nanomaterials), scalability and commercial availability, and operation at room temperature demonstrate its great potential for real applications, especially in PoC devices. Thus, the two-step, ChOx-Fe-BTC-TMB system is successful for detecting cholesterol in the range of 6.56 – 78.75 μM, with an LOD of 2.91 μM and 2.88 μM at ChOx-cholesterol incubation temperatures of 25 ºC and 37 ºC, respectively.

3.5 Selectivity Studies

The selectivity of the ChOx-FeBTC-TMB biosensor system to H_2O_2 and cholesterol detection in the presence of other interferents, commonly found in real blood samples, was investigated.

3.5.1 H_2O_2 Selectivity Studies

The selectivity of Fe-BTC-TMB biosensor to H_2O_2 in the presence of common blood interferents such as amino acids (glycine, L-lysine, L-cysteine), small molecules (urea, uric acid, glucose, sucrose, fructose), salts (KCl, $CaCl_2$, NaCl), and a mixture of these interferents was investigated. The sensor absorbance of H_2O_2 in the presence of interfering analytes is demonstrated in Figure 15. As seen, the Fe-BTC-TMB signal response to H_2O_2 remained relatively constant in the presence of most interfering analytes with slight, insignificant variations. Selectivity to H_2O_2 in the presence of NaCl at concentration equal to and 10x higher than H_2O_2 (the latter mimicking real blood samples) showed minminor change (< 5% suppression). Only L-cysteine caused major suppression to H_2O_2 signal when added alone and in a mixture of interferents, further confirmed by the lack of color change (see insert Figure 15). This is attributed to the reducing nature of L-cysteine, which consumes oxygen and reduces oxTMB [12]. The competing nature was observed in a similar, peroxidase-mimic based cholesterol sensor [12,49]. It is noteworthy that L-cysteine was tested at equal concentrations with H_2O_2. Meanwhile, L-cysteine in real blood samples is usually present at much lower concentrations than that of cholesterol, and blood samples undergo dilution prior to using Fe-BTC-TMB sensor. Hence, the interfering impact of L-cysteine would be much lower in real applications [49]. Moreover, N-ethylmaleimide can be added to eliminate suppression effects by L-cysteine [49,59]. Notably, the standard deviations of all three replicates was low, indicating good repeatability and reliability of the obtained results. Thus, the Fe-BTC-TMB biosensor system is considered to have good selectivity to H_2O_2, with insignificant response to most interferents.

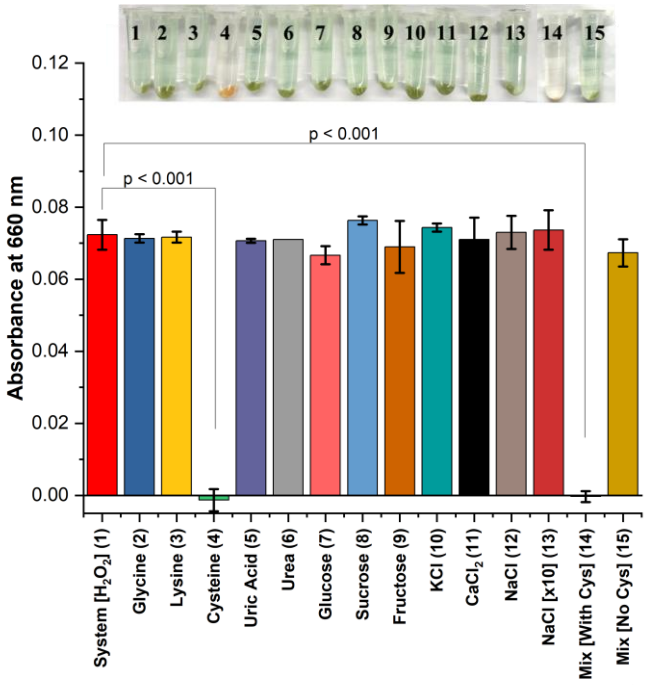

Figure 15: Selectivity of Fe-BTC-TMB system to 40 µM H_2O_2 detection in presence of interfering analytes at 40 µM, except NaCl [x10] was at 400 µM. Error bars represent the standard deviations of three trials. All samples showed insignificant differences in absorption compared to the system sample, with p-values greater than 0.05 – except those labelled. Insert shows the change in color intensity when detecting H_2O_2 in presence of interfering analytes, labelled with numbers corresponding to numbers in x-axis label.

3.5.2 Cholesterol Selectivity Studies

The selectivity of ChOx-Fe-BTC-TMB biosensor to cholesterol in the presence of common blood interferents was further tested, using 37 ºC ChOx-cholesterol incubation temperature, to stress the system and push it to its limit. We note that the selectivity study was conducted on a smaller group of analytes that are likely to interfere with the sensing mechanism, as performed in previous studies [49]. These were L-cysteine, glucose, fructose, uric acid, NaCl at high concentration, and a mixture of these interferents with and without cysteine. The sensor absorbance of cholesterol in the presence of interfering analytes is demonstrated in Figure 16. The ChOx-Fe-BTC-TMB signal response to cholesterol remained relatively constant in the presence of most interfering analytes, with slight variations. Similar to H_2O_2 selectivity, only L-cysteine caused major suppression to the sensor signal when added alone and in a mixture of interferents, further confirmed by the lack of color change (see insert of Figure 16). As discussed earlier, this interfering impact of L-cysteine would be much lower in real applications and can be eliminated by using N-ethylmaleimide [49,59]. Uric acid also caused a slight suppression in the signal, which may be attributed to its reducing nature and possible interactions with the ChOx enzyme. However, the suppression is not statistically significant and is within a tolerable range ($p < 0.001$). Thus, the ChOx-Fe-BTC-TMB biosensor system is considered to have good selectivity to cholesterol, with insignificant response to most interferents. Further studies in real blood samples would provide a more comprehensive understanding of all possible interferents and sensor performance in real-life applications.

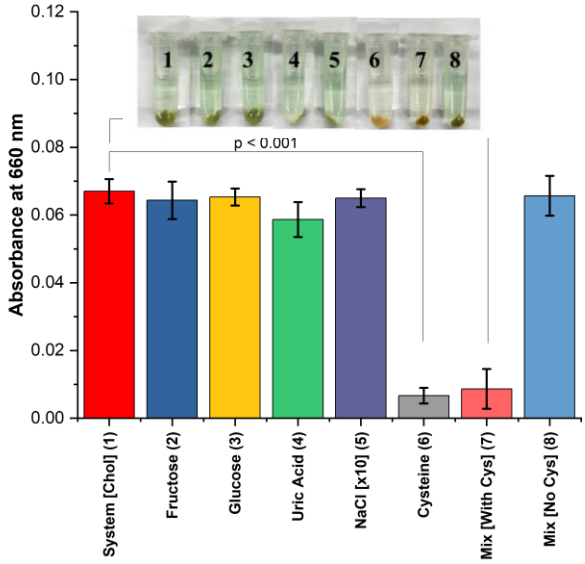

Figure 16: Selectivity of Fe-BTC-TMB system to cholesterol detection in the presence of interfering analytes. Error bars represent the standard deviations of three trials. All samples showed insignificant differences in absorption compared to the system sample, with p-values greater than 0.05, except those labelled. The insert shows the change in color intensity when detecting cholesterol in the presence of interfering analytes, labelled with numbers corresponding to the numbers in the x-axis label.

4. Conclusions

This paper investigated the potential use of Fe-BTC as a novel peroxidase mimic for spectrophotometric detection of cholesterol. Fe-BTC demonstrated effective, intrinsic peroxidase activity, where Fe centers played a key role in facilitating H_2O_2 decomposition and subsequent TMB oxidation. H_2O_2 detection was achieved at an LOD of 3.30 µM, while cholesterol could be detected at concentrations as low as 2.88 µM, at 37 °C incubation temperature. The sensor can detect a wide range of cholesterol concentrations, from 6.56 – 78.75 µM. The biosensing system also demonstrated excellent selectivity to cholesterol in the presence of most interferents. The proposed Fe-BTC-TMB biosensor system for cholesterol detection demonstrates great promise. The novelty of the sensor lies in employing readily accessible Fe-BTC as an efficient nanozyme with strong peroxidase-like activity. Its high catalytic stability and ease of integration into the sensing platform make Fe-BTC an excellent candidate for portable and rapid cholesterol detection. These attributes support the feasibility of developing reliable, low-resource PoC diagnostic systems based on this material. However, one drawback is the use of ChOx enzyme, which may limit storage conditions due to high denaturation susceptibility. To tackle this, future studies can examine the design of enzyme-free biosensors. Future studies can also focus on evaluating the biosensor's performance to accurately quantify cholesterol levels in actual blood samples and explore integration in PoC devices. Overall, the novel Fe-BTC-based biosensor proved effective in cholesterol detection.

Funding

This work was funded by the American University of Sharjah (FRG24-C-E60) and Khalifa University under Award No. FSU-2023-028.

Acknowledgments

The authors gratefully acknowledge the support of the Materials Science Research Center at the American University of Sharjah for conducting the XRD characterization tests.

Data availability

Data are available on request from the corresponding author.

Author Contributions Statement

Heba Abed: Investigation, and writing - original draft. Rana Sabouni: Supervision, project administration, funding, conceptualization, and review and editing. Mehdi Ghommem: Supervision, conceptualization, funding, and review and editing. Muhammad Umar Azam: Investigation, and running characterization tests. Nouha Alcheikh: Resources, funding, and review and editing. Khalid Askar: funding, and review and editing

References

1. Schade, D. S., Shey, L. & Eaton, R. P. Cholesterol Review: A Metabolically Important Molecule. *Endocrine Practice* **26**, 1514–1523 (2020).
2. McNamara, D. J. Cholesterol: Sources, Absorption, Function, and Metabolism. *Encyclopedia of Human Nutrition* **1–4**, 341–345 (2013).
3. Sonal Sekhar, M., Reddy, B. S., Kurian, S. J., Rao, M. & Marupuru, S. Physiological role of cholesterol in human body. *Dietary Sugar, Salt and Fat in Human Health* 453–481 (2020) doi:10.1016/B978-0-12-816918-6.00021-4.
4. Triviño, A. *et al.* Effects of Hypercholesterolaemia in the Retina. *Ocular Diseases* https://doi.org/10.5772/48359 (2012) doi:10.5772/48359.
5. Prasad, K. & Mishra, M. Mechanism of Hypercholesterolemia-Induced Atherosclerosis. *Rev Cardiovasc Med* **23**, 212 (2022).
6. Emanuelsson, F., Nordestgaard, B. G. & Benn, M. Familial Hypercholesterolemia and Risk of Peripheral Arterial Disease and Chronic Kidney Disease. *J Clin Endocrinol Metab* **103**, 4491–4500 (2018).
7. High Cholesterol Facts | Cholesterol | CDC. https://www.cdc.gov/cholesterol/data-research/facts-stats/index.html.
8. Abed, H., Sabouni, R. & Ghommem, M. MOF-based spectrophotometric sensors for cholesterol detection: current trends and challenges. *RSC Adv* **14**, 39472–39497 (2024).
9. Huang, X. *et al.* Advances in metal–organic framework-based nanozymes and their applications. *Coord Chem Rev* **449**, 214216 (2021).

10. Wu, J. *et al.* Nanomaterials with enzyme-like characteristics (nanozymes): next-generation artificial enzymes (II). *Chem Soc Rev* **48**, 1004–1076 (2019).

11. Liu, L. *et al.* Colorimetric Detection of Cholesterol Based on the Peroxidase-Like Activity of Metal-Organic Framework MIL-101(Cr). *ChemistrySelect* **6**, 7143–7149 (2021).

12. Wu, Y. *et al.* Metal-organic framework coated Fe3O4 magnetic nanoparticles with peroxidase-like activity for colorimetric sensing of cholesterol. *Sens Actuators B Chem* **249**, 195–202 (2017).

13. Abdolmohammad-Zadeh, H. & Ahmadian, F. A fluorescent biosensor based on graphene quantum dots/zirconium-based metal-organic framework nanocomposite as a peroxidase mimic for cholesterol monitoring in human serum. *Microchemical Journal* **164**, 106001 (2021).

14. Li, Y. *et al.* Pd Nanoclusters Confined in ZIF-8 Matrixes for Fluorescent Detection of Glucose and Cholesterol. *ACS Appl Nano Mater* **4**, 9132–9142 (2021).

15. Oveisi, A. R., Khorramabadi-Zad, A. & Daliran, S. Iron-based metal–organic framework, Fe(BTC): an effective dual-functional catalyst for oxidative cyclization of bisnaphthols and tandem synthesis of quinazolin-4(3H)-ones. *RSC Adv* **6**, 1136–1142 (2015).

16. Sciortino, L., Alessi, A., Messina, F., Buscarino, G. & Gelardi, F. M. Structure of the FeBTC metal-organic framework: A model based on the local environment study. *Journal of Physical Chemistry C* **119**, 7826–7830 (2015).

17. Fonseca, J., Gong, T., Jiao, L. & Jiang, H. L. Metal–organic frameworks (MOFs) beyond crystallinity: amorphous MOFs, MOF liquids and MOF glasses. *J Mater Chem A Mater* **9**, 10562–10611 (2021).

18. Ye, Q. *et al.* Incorporation of Fluorescent Carbon Quantum Dots into Metal–Organic Frameworks with Peroxidase-Mimicking Activity for High-Performance Ratiometric Fluorescent Biosensing. *J Anal Test* **7**, 16–24 (2023).

19. Yang, H. *et al.* A bimetallic (Co/2Fe) metal-organic framework with oxidase and peroxidase mimicking activity for colorimetric detection of hydrogen peroxide. *Microchimica Acta* **184**, 4629–4635 (2017).

20. Shrivastava, A. & Gupta, V. B. Methods for the determination of limit of detection and limit of quantitation of the analytical methods. *Chronicles of Young Scientists* **2**, 21 (2011).

21. Araya, T. *et al.* Selective degradation of organic dyes by a resin modified Fe-based metal-organic framework under visible light irradiation. *Opt Mater (Amst)* **64**, 512–523 (2017).

22. Said, M. I., Abd EL-Wahab, M. M. & Sadek, A. M. FeBTC MOF-Derived Fe3O4@C Nanocomposite: Controlled Synthesis and Application as Potential Adsorbent for Rhodamine Dye Elimination From Wastewater. *Appl Organomet Chem* **39**, e7869 (2025).

23. Kim, D., Koo, K. C., Park, J. H., Paeng, K. & Lee, W. Roll-to-Roll Processing of Hybrid MOF and Nylon Membranes for High Efficiency Removal of Toxic Gases, Heavy Metals, and Dyes. *ACS Applied Engineering Materials* **1**, 1220–1228 (2023).

24. Siew, W. Y., Abu Bakar, N. H. H., Abu Bakar, M. & Zainal Abidin, A. Influence of various Cu/Fe ratios on the surface properties of green synthesized Cu-Fe-BTC and it`s relation to methylene blue adsorption. *J Hazard Mater* **416**, 125846 (2021).

25. Ferraz, H. C., Guimarães, J. A., Alves, T. L. M. & Constantino, C. J. L. Monomolecular films of cholesterol oxidase and S-Layer proteins. *Appl Surf Sci* **257**, 6535–6539 (2011).

26. Bianchetti, M. G. & Bettinelli, A. Differential Diagnosis and Management of Fluid, Electrolyte, and Acid–Base Disorders. *Comprehensive Pediatric Nephrology: Text with CD-ROM* 395–431 (2008) doi:10.1016/B978-0-323-04883-5.50033-7.

27. García, E. R. *et al.* Adsorption of Azo-Dye Orange II from Aqueous Solutions Using a Metal-Organic Framework Material: Iron- Benzenetricarboxylate. *Materials 2014, Vol. 7, Pages 8037-8057* **7**, 8037–8057 (2014).

28. Moloto, W., Mbule, P., Nxumalo, E. & Ntsendwana, B. Enhanced optical and electrochemical properties of FeBTC MOF modified TiO2 photoanode for DSSCs application. *Scientific Reports 2024 14:1* **14**, 1–14 (2024).

29. Hamid, M. & Khalil-ur-Rehman. Potential applications of peroxidases. *Food Chem* **115**, 1177–1186 (2009).

30. Thakur, B. *et al.* An Investigation into the Intrinsic Peroxidase-Like Activity of Fe-MOFs and Fe-MOFs/Polymer Composites. *Adv Mater Technol* **6**, 2001048 (2021).

31. Ji, L. *et al.* Facile synthesis of Fe-BTC and electrochemical enhancement effect for sunset yellow determination. *Talanta Open* **5**, 100084 (2022).

32. Castañeda-Ramírez, A. A. *et al.* Magnetite nanoparticles into Fe-BTC MOF as adsorbent material for the remediation of metal (Cu(II), Pb(II, As(III) and Hg(II)) ions-contaminated water. *Catal Today* **394–396**, 94–102 (2022).

33. Devarajan, N. & Suresh, P. Iron-MOF-Catalyzed Domino Cyclization and Aromatization Strategy for the Synthesis of 2,4-Diarylquinolines. *Asian J Org Chem* **9**, 437–444 (2020).

34. Said, M. I., Abd EL-Wahab, M. M. & Sadek, A. M. FeBTC MOF-Derived Fe3O4@C Nanocomposite: Controlled Synthesis and Application as Potential Adsorbent for Rhodamine Dye Elimination From Wastewater. *Appl Organomet Chem* e7869 (2024) doi:10.1002/AOC.7869.

35. Kim, D., Kim, I. J., Kwon, H. T., Paeng, K. & Lee, H. CuBTC Metal-Organic Framework Decorated with FeBTC Nanoparticles with Enhance Water Stability for Environmental Remediation Applications. *ACS Omega* **8**, 14900–14906 (2023).

36. Patravale, V., Dandekar, P. & Jain, R. Characterization techniques for nanoparticulate carriers. *Nanoparticulate Drug Delivery* 87–121 (2012) doi:10.1533/9781908818195.87.

37. Xu, R. Progress in nanoparticles characterization: Sizing and zeta potential measurement. *Particuology* **6**, 112–115 (2008).

38. Goldstein, N. & Greenlee, L. F. Influence of synthesis parameters on iron nanoparticle size and zeta potential. *Journal of Nanoparticle Research* **14**, 1–15 (2012).

39. Hirschle, P. *et al.* Exploration of MOF nanoparticle sizes using various physical characterization methods – is what you measure what you get? *CrystEngComm* **18**, 4359–4368 (2016).

40. Araya, T. *et al.* Selective degradation of organic dyes by a resin modified Fe-based metal-organic framework under visible light irradiation. *Opt Mater (Amst)* **64**, 512–523 (2017).

41. Moloto, W., Mbule, P., Nxumalo, E. & Ntsendwana, B. Enhanced optical and electrochemical properties of FeBTC MOF modified TiO2 photoanode for DSSCs application. *Scientific Reports 2024 14:1* **14**, 1–14 (2024).

42. Pellenz, L. *et al.* A comprehensive guide for characterization of adsorbent materials. *Sep Purif Technol* **305**, 122435 (2023).

43. Saha, S. *et al.* Design of Dual Purpose Fe-metallogel for Magnetic Refrigeration and Fabrication of Schottky Barrier Diode. *ChemistrySelect* **7**, e202203307 (2022).

44. Otuzoğlu, J. & Demircan, O. The Utilization of Bimetallic Fe–Co Metal Organic Framework as a Catalyst for the Oxygen Reduction Reaction in Microbial Fuel Cells Cathode. *J Inorg Organomet Polym Mater* 1–10 (2024) doi:10.1007/S10904-024-03502-9/FIGURES/7.

45. Dolz, M. *et al.* The colors of peroxygenase activity: Colorimetric high-throughput screening assays for directed evolution. *Methods Enzymol* **693**, 73–109 (2023).

46. Péter, T. *et al.* Correlations Between Colloidal Stability and Peroxidase Activity of Prussian Blue Nanozymes in Salt Solutions. *J Phys Chem B* **129**, 6879–6885 (2025).

47. Li, S. *et al.* Enhanced peroxidase-like activity of MOF nanozymes by co-catalysis for colorimetric detection of cholesterol. *J Mater Chem B* **11**, 7913–7919 (2023).

48. Overview: High cholesterol - InformedHealth.org - NCBI Bookshelf. https://www.ncbi.nlm.nih.gov/books/NBK279318/.

49. Chen, P. *et al.* Au/CeO2NR Restricted Inside Cu-MOFs: A Three-in-One Artificial Enzyme with Synergistically Enhanced Peroxidase-Like Activity for Dual-Mode Sensing of Multiple Biomarkers. *ACS Sustain Chem Eng* **11**, 8106–8119 (2023).

50. Xu, D. *et al.* MOF@MnO2 nanocomposites prepared using in situ method and recyclable cholesterol oxidase–inorganic hybrid nanoflowers for cholesterol determination. *Nanotechnology* **32**, 315502 (2021).

51. Hassanzadeh, J., Khataee, A. & Eskandari, H. Encapsulated cholesterol oxidase in metal-organic framework and biomimetic Ag nanocluster decorated MoS2 nanosheets for sensitive detection of cholesterol. *Sens Actuators B Chem* **259**, 402–410 (2018).

52. Xu, X., Zhao, Y., Tan, H., Ma, Y. & Li, Y. In situ encapsulation of horseradish peroxidase in zeolitic imidazolate framework–8 enables catalyzing luminol reaction under near-neutral conditions for sensitive chemiluminescence determination of cholesterol. *Microchimica Acta* **187**, 1–8 (2020).

53. Gong, M., Yang, J., Li, Y., Zhuang, Q. & Gu, J. Substitution-type luminescent MOF sensor with built-in capturer for selective cholesterol detection in blood serum. *J Mater Chem C Mater* **7**, 12674–12681 (2019).

54. Wu, Y. *et al.* Optimization of the tandem enzyme activity of V-MOF and its derivatives for highly sensitive nonenzymatic detection of cholesterol in living cells. *J Colloid Interface Sci* **649**, 601–615 (2023).

55. Amirzehni, M., Eskandari, H., Vahid, B. & Hassanzadeh, J. An efficient chemiluminescence system based on mimic CuMOF/Co3O4 nanoparticles composite for the measurement of glucose and cholesterol. *Sens Actuators B Chem* **348**, 130690 (2021).

56. Zhao, M., Li, Y., Ma, X., Xia, M. & Zhang, Y. Adsorption of cholesterol oxidase and entrapment of horseradish peroxidase in metal-organic frameworks for the colorimetric biosensing of cholesterol. *Talanta* **200**, 293–299 (2019).

57. Ding, J. *et al.* Highly dispersive AuNCs/ChOx@ZIF-8/PEI nanocomplexes for fluorescent detection of cholesterol in human serum. *Microchimica Acta* **189**, 1–10 (2022).

58. MIL-101 (Cr) - CD Bioparticles. https://www.cd-bioparticles.net/p/9151/mil-101-cr?srsltid=AfmBOooyHRcVVid6KwD8bclGQ5LMYC0fQIrRxaNFVEhRO6xQzubzHf9U.

59. Zhou, X., Wang, M., Chen, J., Xie, X. & Su, X. Peroxidase-like activity of Fe–N–C single-atom nanozyme based colorimetric detection of galactose. *Anal Chim Acta* **1128**, 72–79 (2020).